PERGAMON

Aerosol Science 33 (2002) 519–531

Journal of
Aerosol Science

www.elsevier.com/locate/jaerosci

The influence of operating parameters on number-weighted aerosol size distribution generated from a gas metal arc welding process

Anthony T. Zimmer[a,*], Paul A. Baron[a], Pratim Biswas[b]

[a] *National Institute for Occupational Safety and Health, Division of Applied Research and Technology, 4676 Columbia Parkway, Cincinnati, OH 45226, USA*

[b] *Washington University, Departments of Chemical and Civil Engineering, One Brookings Drive, Campus Box 1180, St. Louis, MO 63130-4899, USA*

Received 10 May 2001; received in revised form 27 September 2001; accepted 28 September 2001

Abstract

In light of recent research on the potential health problems associated with sub-micrometer aerosols, a study was conducted to determine the effect that droplet mass transfer mode, shield gas composition, and welding spatter had upon the aerosols generated from a Gas Metal Arc Welding (GMAW) Operation. The results revealed that the sub-micrometer aerosols produced during spray transfer resulted in markedly higher concentrations of nucleated particles than those produced during globular transfer. This probably resulted from a larger droplet surface area for vaporization of metallic species. The shield gas experiments results revealed that as the percentage of carbon dioxide increased the number of nucleated particles also increased. It appears that oxygen may have facilitated chemical reactions with the alloy constituents, thereby increasing the mass transfer rate from the evaporating metal droplets in the plasma. Finally, an attempt to characterize the spatter aerosol revealed a distinct particle size distribution with a mode particle diameter of 6.8 μm. This particle size distribution appeared to be independent of shield gas composition, and the particle number concentration was significantly smaller than the sub-micrometer aerosols formed during the GMAW process (i.e., two-orders of magnitude smaller when weighted by particle mass). Published by Elsevier Science Ltd.

Keywords: Welding; Fumes; Arc; Spatter

* Corresponding author. Tel.: +1-513-841-4370; fax: +1-513-841-4500.
E-mail address: atz0@cdc.gov (A.T. Zimmer).

0021-8502/02/$ - see front matter. Published by Elsevier Science Ltd.
PII: S0021-8502(01)00189-6

1. Introduction

Census data indicates that over 600,000 workers in the United States are involved in welding or allied processes. Animal and epidemiological studies suggest that welding is associated with a wide range of adverse health effects such as metal fume fever, pneumonitis, chronic bronchitis, and decrements in pulmonary function (NIOSH, 1988). Welding processes are known to generate sub-micrometer sized aerosols, and recent research has indicated sub-micrometer aerosols may cause adverse health effects due to their size (Ferin et al., 1990; Oberdorster et al., 1990; Takenaka, Dornhofer-Takenaka, & Muhle, 1986). This research suggests that a lower moment of the particle size distribution (e.g., particle number or particle surface area) may be more toxicologically relevant.

Welding processes are known to generate high fume formation rates (FFR) with values typically ranging from 1.7 to 8.3 mg s^{-1} (Gray & Hewitt, 1982; Heile & Hill, 1975; Hewitt & Hirst, 1993; Hilton & Plumridge, 1991). In light of mass-based occupational safety and health standards, prior welding research has primarily focused upon characterizing how various welding parameters affect the FFR to indicate the relative cleanliness of a welding process. Gas Metal Arc Welding (GMAW) processes, frequently encountered in the welding industry, use filler metals (welding alloys) that require shield gases (e.g., argon/carbon dioxide gases) to protect the molten metals within the arc against oxidation and to provide the desired arc characteristics (Fig. 1). Prior research has demonstrated that several parameters affect the FFR of GMAW processes including the mass transfer mode of molten droplets within the arc, the shield gas composition, and welding spatter (Gray & Hewitt, 1982; Heile & Hill, 1975; Hewitt & Hirst, 1993; Hilton & Plumridge, 1991).

In GMAW processes, welding professionals typically operate using two modes of droplet metal transfer across the arc and these modes are termed globular and spray transfer (Heile & Hill, 1975; Hilton & Plumridge, 1991; Ma & Apps, 1982). Globular droplet transfer is typically associated with low applied currents and have the following characteristics: a diffuse arc with the root covering all of the globule surface, high electrical resistance with a calculated mean droplet temperature of $\sim 2750^{\circ}$C, and enhanced transfer of the metal vapors resulting in *high fume generation rates* (Ma and Apps, 1982). Spray droplet transfer is associated with high applied currents and has the following characteristics: a conical arc that surrounds the column of irregularly shaped/sized metal droplets, high electrical resistance with a calculated mean droplet temperature of $\sim 2750^{\circ}$C, enhanced transfer of metal vapors resulting in *high fume generation rates* (Ma and Apps, 1982).

The shield gas composition also influences the fume formation rate in GMAW processes. Typically, an oxidizing gas, such as carbon dioxide and oxygen, is used to assist in arc stability. In GMAW operations involving argon/carbon dioxide/oxygen mixtures, an increase in the percentage of oxygen increased the FFR (Heile & Hill, 1975; Hilton & Plumridge, 1991). For example, the FFR for a GMAW operation involving mild steel solid wires welded at 300 A increased from 2.7 mg s^{-1} using a shield gas composed of 93% Ar, 5% CO_2, 2% O_2 to 4.5 mg s^{-1} using a more oxidizing shield gas composed of 78% Ar, 20% CO_2, 2% O_2. Additionally, when pure CO_2 was used the FFR markedly increased to 7.3 mg s^{-1} (Hilton & Plumridge, 1991). Prior research has also shown that an increase in oxidizing gases in the shield gas will increase spatter formation (Gray, Hewitt, & Dare, 1982; Hewitt & Hirst, 1993). High spatter emissions are considered undesirable because of the potential for occupational injury due to skin burns.

The formation of welding spatter can also have a significant effect on the composition of the fume and its rate of formation. During welding, spatter is associated with an unstable arc condition

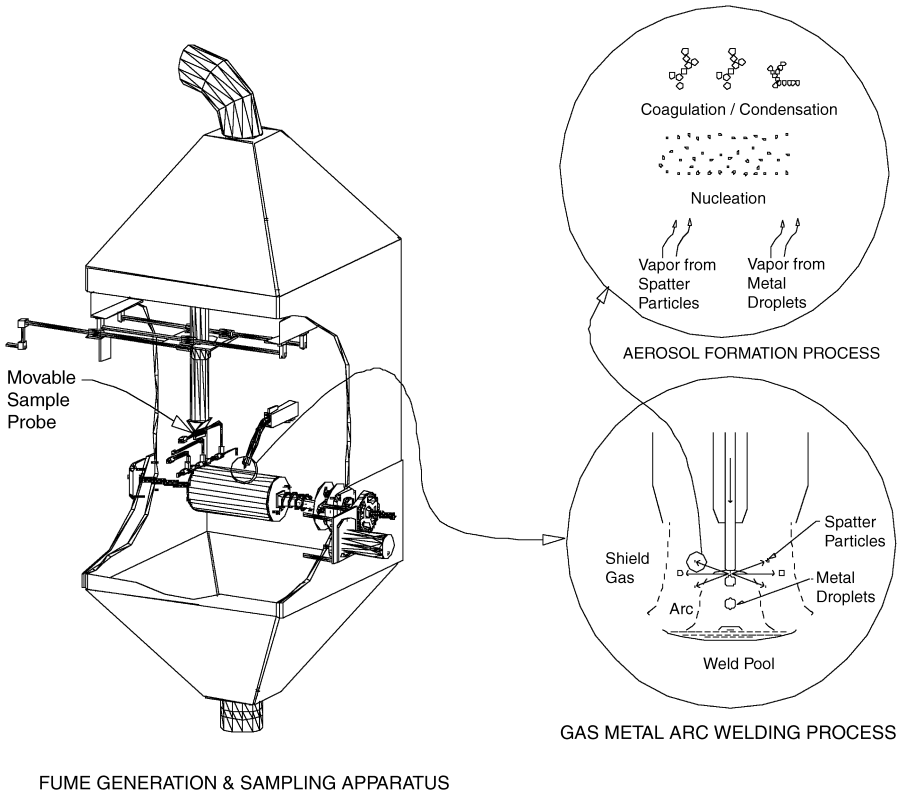

Fig. 1. Schematic illustration: (1) the fume generation and sampling apparatus, (2) the operation of the GMAW process, and (3) the probable formation of aerosols during a GMAW process.

and a turbulent weld-pool (Hewitt & Hirst, 1993). In GMAW processes, the electrical current is delivered through the filler wire. As the filler wire constricts during droplet separation, the current density in the reducing cross section increases until separation occurs explosively (Gray, Hewitt, & Hicks, 1980). This results in the almost instantaneous evaporation of some of the remaining metal filament and the ejection of a spray of very hot metal droplets called spatter. Spatter ejected this way, and by other arc forces, represents a large surface area from which further evaporation can occur and increase the formation of fumes. It was experimentally shown that at least 25% of the fume from solid wire GMAW welding originated from outside of the arc region (Gray, 1980b), and that an increase in oxidizing gases in the shield gas will increase spatter formation (Gray et al., 1982; Hewitt & Hirst, 1993). However, it is thought that the ejected spatter particles are too large to remain airborne and do not contribute directly to the fume (Gray, 1980a; Hewitt & Hirst, 1993).

Although the effect of mass transfer mode, shield gas composition, and welding spatter on the mass-based fume formation rate is known, no information is available on how these factors affect the resultant particle size distribution, especially particle size distributions weighted by particle number or particle surface area. In light of recent research on the potential health problems associated with sub-micrometer aerosols, an apparatus was designed to characterize aerosols generated from GMAW and other welding processes based upon particle number (Zimmer & Biswas, 2001). The results

demonstrated that the aerosols generated from these processes were multi-modal and temporally changing. In this paper, the role of mass transfer of molten droplets through the plasma, shield gas composition, and welding spatter on the resultant particle number size distribution is established.

2. Experimental

An experimental apparatus (Fig. 1) was designed to promote the steady-state generation of welding fumes over a period of several minutes and details are provided in an earlier paper (Zimmer & Biswas, 2001). A high quality, commercial arc welding system (Miller Deltaweld Series 452 power source and Miller S-62 wire feeder) was selected to generate GMAW aerosols. In this setup, wire alloy, fed at a constant speed, provided the filler material for the arc welding process. Within the high-temperature regime of the arc, the solid wire transformed into superheated metal droplets that deposited onto a mild steel cylindrical substrate (16.8 cm diameter, 0.66 cm thickness, ASTM A-53-B grade steel) (Fig. 1). A low speed motor, located outside of the chamber, was used to rotate the cylinder at constant speed of 0.63 cm s^{-1}. The thread pitch of the Acme screw determined the distance between the overlapping weld bead (0.25 cm). Shield gases were used to stabilize the arc and to prevent chemical oxidation of the molten metal droplets and molten substrate. The shield gases, composed of argon and carbon dioxide, were metered to the welding unit using mass flow controllers (Unit Instruments Inc., Orange, CA, Model UFC-1100). This allowed flexibility in controlling the shield gas flowrate and composition. Metal fumes were generated from an arc welding process directly from volatilization of the metal vapor from the superheated molten droplets, and indirectly from spatter particles ejected during the welding process (Gray & Hewitt, 1982) (Fig. 1). HEPA-filtered, particle-free air was pulled up vertically through the chamber using an industrial air cleaner (ACE Corp, Model 73-800G) with a constant volumetric flowrate of 4.55×10^4 cm^3 s^{-1} and an average velocity through the chamber of 6.1 cm s^{-1}. Honeycomb flow-straighteners were used to smooth the air prior to reaching the cylindrical substrate. The fume laden air was filtered, using 95% efficiency filters, prior to being exhausted to the outside.

The welding process generated an aerosol-laden plume that mixed with the HEPA filtered air. A movable sampling probe was used to collect fume samples for aerosol measurements (Fig. 1). The probe, a modified design from Biswas (1993), allowed for accurate sample collection in both the horizontal and vertical directions relative to the arc location. Cylindrical symmetry, about a vertical axis centered on the weld site, was assumed. Samples were collected isoaxially, although not isokinetically. Due to the small Stokes number of welding aerosols (<0.01), isokinetic losses are expected to be negligible (Hinds, 1999). Because of the high number concentrations encountered during this process, a dual-stage dilution system was designed to allow up to a 1000-fold decrease in the particle number concentration. This design served to quench chemical and aerosol dynamic processes within the sample line to allow collection of representative samples. The modified sample probe significantly reduced the time for second stage dilution from a second to millisecond timescale (Zimmer & Biswas, 2001).

Several aerosol instruments were used to evaluate the particle size distribution of the welding aerosol. Following dilution, sub-micrometer aerosol measurements were made by directing a portion of the diluted sample to a Scanning Mobility Particle Sizer (SMPS) (TSI Inc., an Electrostatic Classifier, Model 3080, using either a Long Differential Mobility Analyzer (DMA), Model 3081 or

Table 1
Experimental plan to evaluate effect of various welding parameters on the particle size distribution

	Welding conditions		Aerosol measurement technique[a]		
Welding parameter studied	Arc voltage	Extension height (cm)	SMPS/Long DMA	SMPS/Nano DMA	Aerosizer
Mass transfer mode					
Globular	20.5	1	3	3	
Spray	30.5	1.5	4	4	
Shield gas composition					
90% Ar/10% CO_2	20.5	1	3	3	
80% Ar/20% CO_2	20.5	1	3	3	
0% Ar/100% CO_2	20.5	1	3	3	
Welding spatter					
90% Ar/10% CO_2	20.5	1			2
0% Ar/100% CO_2	20.5	1			2

[a]Note: numbers represent the number of replicate sample runs conducted; composition is percent by volume; SMPS—Scanning Mobility Particle Sizer; DMA—Differential Mobility Analyzer.

a Nano Differential Mobility Analyzer, Model 3085, and a Condensation Particle Counter, Model 3022A operated in the scanning mode). To determine if welding spatter generated a measurable micrometer-scaled aerosol, an Aerosizer (TSI Inc., Model 3220) was used. Condensation Particle Counter (CPC) (TSI Inc., Model 3022A) measurements had been previously taken to confirm that the aerosol concentration fluctuated little over the time-scales required to obtain particle size distribution measurements (Zimmer & Biswas, 2001).

Conditions that were held constant in this work included: the wire alloy (according to the material safety data sheet, this alloy is composed of 97.5% iron, 1.2–1.6% manganese, 0.8–1.0% silica, and 0.1% copper), the welding substrate (ASTM A-53-B grade steel), the wire feed speed (16.1 cm s^{-1}), the volumetric flowrate of the shield gas (0.3 cm^3 s^{-1}), the linear travel speed of the rotating substrate (0.63 cm s^{-1}), and the average velocity of the HEPA-filtered air moving upward through the fume generation chamber (6.1 cm s^{-1}). Conditions that were varied in this work include: the applied arc voltage (to vary the mass transfer mode of molten droplets within the arc), the extension height (distance between the arc welding gun and the substrate), and the shield gas composition (to vary the amount of carbon dioxide available for chemical reactions with the alloy vapors within the arc). Table 1 details the experimental plan used to carry out this study.

3. Results and discussion

3.1. The effect of mass transfer on the particle size distribution of sub-micrometer aerosols

To characterize the effect that the mass transfer mode had on the sub-micrometer particle size distribution, SMPS measurements were taken during globular and spray transfer (Table 1). These

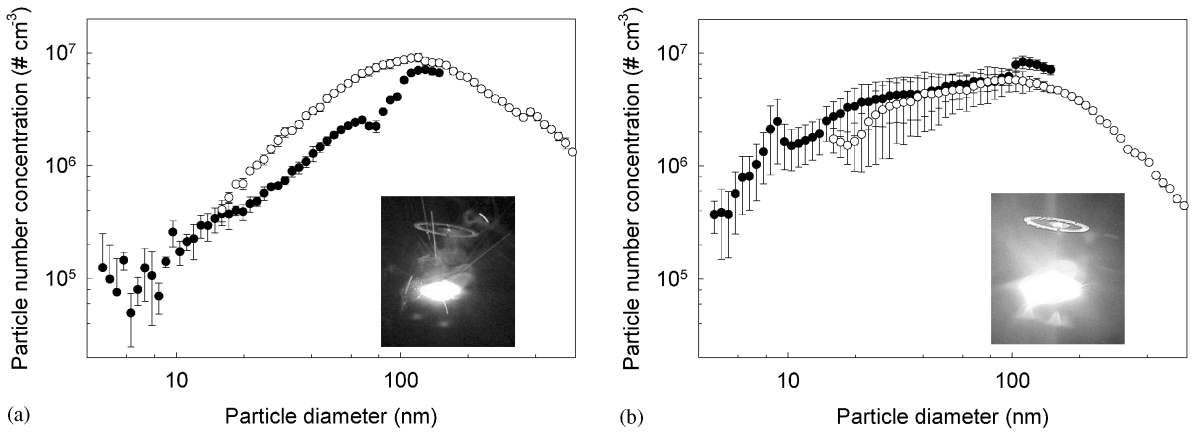

Fig. 2. Scanning Mobility Particle Sizer results for GMAW alloy: (a) during globular transfer mode, and (b) spray transfer mode at a sample height 19.2 cm above the arc centerline using both a Nano DMA (darkened circles, 4.53 nm $< d_p <$ 153 nm) and Long DMA (hollow circles, 16.5 nm $< d_p <$ 562 nm) (note: images on each graph are the arcs corresponding to each mode of metal transfer).

modes were studied because they represent those typically used by welding professionals. During the globular mass transfer, the extension height was 1.0 cm, and the applied arc voltage was 20.5 V (the current during these measurements varied between 194 and 196 A). During the spray mode of metal transfer, the extension height and applied arc voltage was increased to 1.5 cm and 30.5 V (the current during these measurements varied between 180 and 182 A), respectively. Measurements were collected on the arc centerline at a vertical distance of 19.2 cm with a corresponding residence of approximately 3.2 s (i.e., time for a parcel of air to travel from the arc to the sample probe). The dilution system was set to reduce the number concentration of the aerosol entering the probe by 150-fold.

Fig. 2a and b shows the particle number size distributions obtained during the two modes of metal transfer. Three replicate samples were collected for the globular transfer mode while four replicate samples were collected during the spray transfer mode (due to the increased run-to-run variability). The symbols represent the replicate means while the bars represent the standard error associated with each particle-size bin. During each transfer mode, the SMPS was configured using both the Nano DMA (4.53 nm $< d_p <$ 153 nm) and Long DMA (16.5 nm $< d_p <$ 562 nm) to extend the range of the particle diameters studied. When comparing the standard errors between the two modes of metal transfer (Fig. 2a and b), the spray transfer mode had increased variability. A possible reason for this observation may relate to observations made during these experiments. During the experimental runs involving the globular transfer, the arc welding process produced a smooth, consistent bead, resulting in little run-to-run variation. In contrast, the experimental runs during spray transfer resulted in a more diffuse, inconsistent bead that tended to degrade in quality with each bead overlap. This variable bead quality also may have resulted in increased run-to-run variability.

Several observations can be made regarding the total number concentration for the two modes of metal transfer (Fig. 2a and b). The Long DMA results for globular and spray transfer were

similar ($N_{tot} = 6.80 \times 10^6$ and 5.39×10^6 cm^{-3}, respectively). The Nano DMA results for particle sizes less than 16.5 nm indicate that the particle number concentration was one order of magnitude lower for globular transfer (8.1×10^4 versus 8.2×10^5 cm^{-3}). The spray transfer mode probably produces a higher concentration of nucleated particles, resulting from a larger droplet surface area for vaporization of metallic species. Considering the similarities in the droplet temperature (Ma & Apps, 1982), this assumption appears reasonable and is supported by images taken during each mode of metal transfer (Fig. 2a and b). Visible arcs are formed largely by incandescent current-carrying metal vapor (Ma & Apps, 1982). The images of the arcs during each mode of metal transfer show that the spray transfer mode had a larger visible arc when compared to the globular transfer mode (Fig. 2a and b). As a result, arc welding during spray transfer results in a higher number concentration of nucleated particles such that the particle size distribution, sampled at a residence time corresponding to 3.2 s, revealed a distinct accumulation mode and nucleation mode. In contrast, arc welding during globular transfer resulted in a lower number concentration of nucleated particles such that the particle size distribution, at this residence time, revealed only an accumulation mode. The nucleation mode was not apparent because this mode appears to have been already scavenged by larger particles found in the accumulation mode.

Particle statistics are based on the SMPS software package. For both the Nano and Long DMAs, the geometric mean particle sizes for globular transfer were larger than spray transfer. In contrast, the geometric standard deviation for globular transfer was smaller than spray transfer, a result that becomes more pronounced when using the Nano DMA. For example, the geometric mean particle diameter (d_{gm}) for globular and spray transfer using the Long DMA was 113.3 (geometric standard deviation, $\sigma_g = 2.09$) and 89.34 nm ($\sigma_g = 2.19$), respectively. It should be noted that these values represent average values from the replicate sample runs. Similarly, the geometric mean particle diameter for globular and spray transfer using the Nano DMA was 78.28 ($\sigma_g = 1.90$) and 51.22 nm ($\sigma_g = 2.25$), respectively. The apparent increase in the geometric standard deviation for spray transfer may relate to the distinct presence of both an accumulation and nucleation mode that serves to increase dispersion. The Nano DMA for the spray transfer experiments revealed the presence of a distinct nucleation mode with the following particle size statistics for particle diameters in the range of 4.53–16.5 nm: $N_{tot} = 9.45 \times 10^5$ cm^{-3}, $d_{gm} = 10.71$ nm, and $\sigma_g = 1.38$. The particle size distribution for globular transfer suggests that an indistinct nucleation mode may also occur within this range (Fig. 2b).

The experimental results for spray transfer (Fig. 2b) were plotted with a fitted bimodal particle size distribution (using a log-normal assumption) as a comparison (Fig. 3a). The means of the Nano DMA results ($4.53 \text{ nm} < d_p < 16.5 \text{ nm}$) were combined with the means from the Long DMA results ($17.8 \text{ nm} < d_p < 562 \text{ nm}$). The bimodal distribution, determined using a trial and error method, revealed fitted particle size statistics that were quite similar to the experimental results for spray transfer. For example, experimental results for the nucleation mode, using the Nano DMA, compared quite well to the fitted results: $N_{tot,experiment} = 9.45 \times 10^5$ cm^{-3} versus $N_{tot,theory} = 8.0 \times 10^5$ cm^{-3}, $d_{gm,experiment} = 10.7$ nm versus $d_{gm,theory} = 11$ nm, $\sigma_{g,experiment} = 1.38$ versus $\sigma_{g,theory} = 1.4$. The experimental results for the accumulation mode for the Long DMA also compared well to the fitted results: $N_{tot,experiment} = 5.39 \times 10^6$ cm^{-3} versus $N_{tot,theory} = 5.0 \times 10^6$ cm^{-3}, $d_{gm,experiment} = 89.34$ nm versus $d_{gm,theory} = 90$ nm, $\sigma_{g,experiment} = 2.19$ versus $\sigma_{g,theory} = 2.3$.

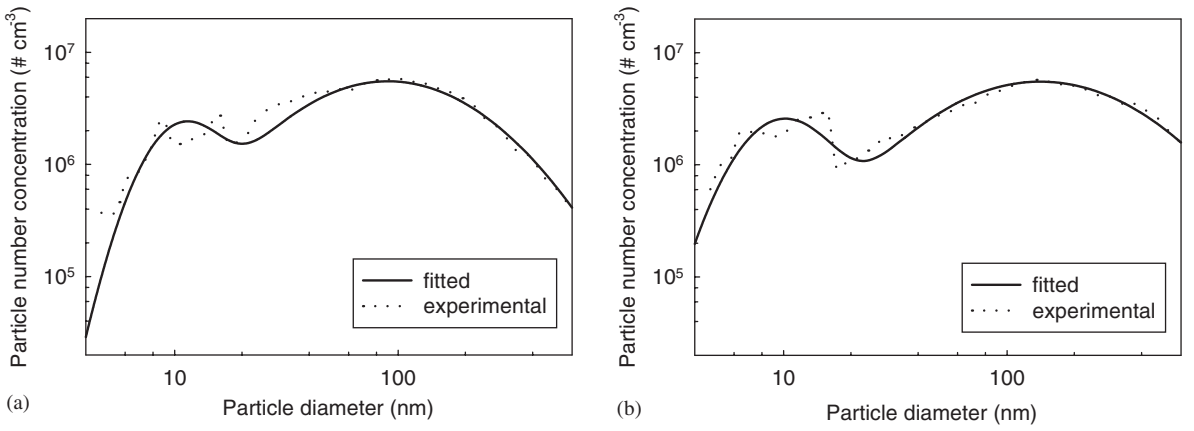

Fig. 3. Comparison of SMPS experimental results to a fitted, bimodal particle size distribution (log-normal): (a) for spray transfer mode, and (b) using 100% CO_2 shield gas (note: experimental results represent mean values that were taken Figs. 2a and 4c).

3.2. The effect of shield gas composition on the particle size distribution of sub-micrometer aerosols

To characterize the effect that the shield gas composition had on the sub-micrometer particle size distribution, SMPS measurements were taken for three shield gas compositions are presented in Table 1. These compositions represent those frequently used by the welding industry. During these experiments, the following conditions were held constant: an extension height of 1.0 cm, an applied arc voltage was 20.5 V (the current during these measurements varied between 194 and 196 A), and a shield gas flowrate of 18 lpm. SMPS measurements were collected on the arc centerline at a vertical distance of 19.2 cm (corresponding residence of approximately 3.2 s), and the dilution system was set to reduce the number concentration of the aerosol entering the probe by 150-fold. Fig. 4a–c shows the particle number size distributions obtained while using different shield gas compositions. Three replicate samples were collected for each experimental condition. During each shield gas condition, the SMPS was configured using both the Nano DMA ($4.53\,\text{nm} < d_p < 153\,\text{nm}$) and Long DMA ($16.5\,\text{nm} < d_p < 562\,\text{nm}$) to extend the range of the particle diameters studied. Several general observations are apparent from Fig. 4a–c. The replicate samples for each experimental condition and each DMA appear reproducible, although the variability increases as the particle diameter decreases. This is reasonable in that the particle counting efficiency decreases with decreasing particle size due to diffusional losses. The results for both the Nano and Long DMA qualitatively appear to agree with one another, although the Long DMA results appear to be smoother. As the percentage of carbon dioxide increases, the number concentration of small diameter particles appears to increase markedly. The availability of oxygen may facilitate chemical reactions with the alloy constituents, thereby increasing the apparent mass transfer rate from the evaporating metal droplets in the plasma. A probable pathway is the reaction of elemental iron to form iron oxide (i.e., FeO), a substance with a significantly higher vapor pressure. Thermodynamic equilibrium calculations were performed to determine the chemical speciation of the elemental and oxide forms of iron at high temperatures (Zimmer, 2000). The results revealed that gaseous FeO would have been the predominant chemical

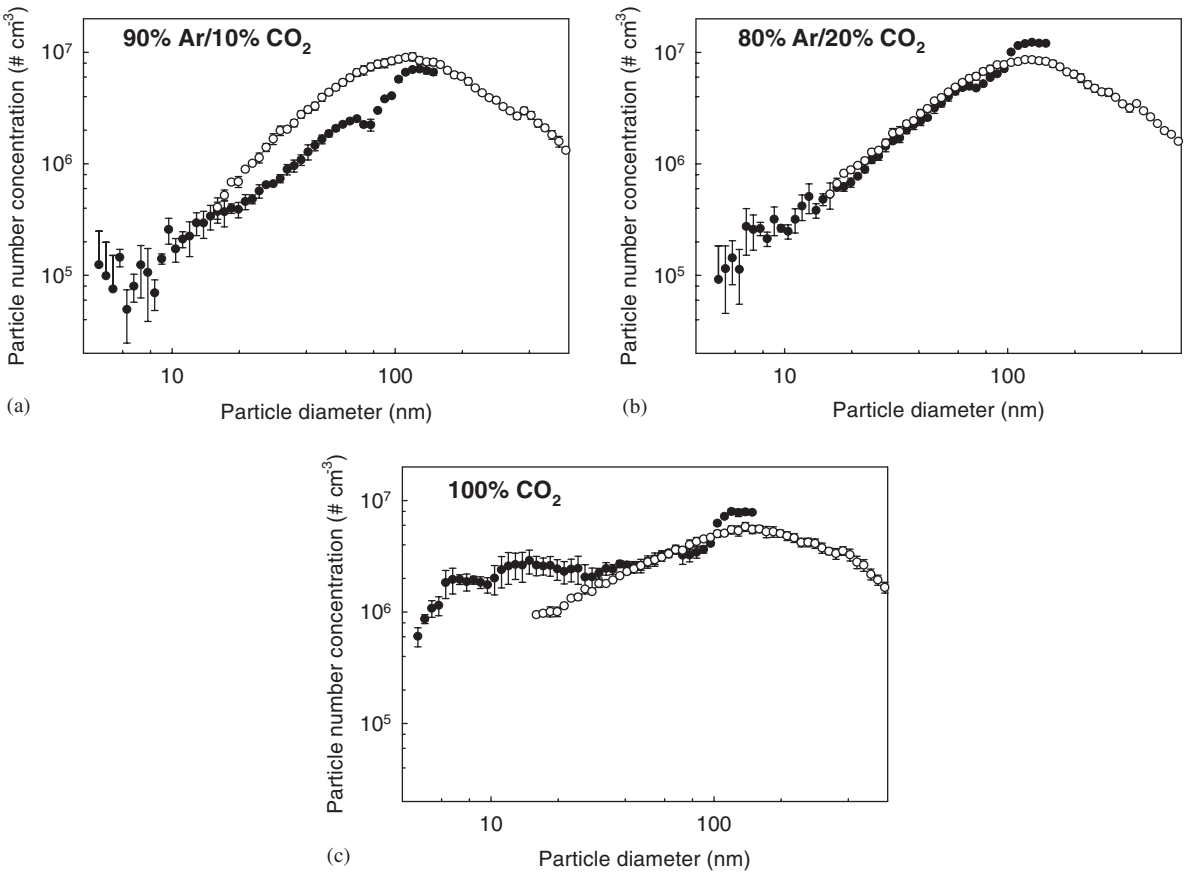

Fig. 4. Scanning Mobility Particle Sizer results for GMAW alloy: (a) using a 90% Ar/10% CO_2 shield gas, (b) 80% Ar/20% CO_2 shield gas, and (c) 100% CO_2 shield gas at a sample height 19.2 cm above the arch centerline using both a Nano DMA (darkened circles, 4.53 nm $< d_p <$ 153 nm) and Long DMA (hollow circles, 16.5 nm $< d_p <$ 562 nm).

species from 2225°C to 2625°C. Therefore, it is probable that, at higher CO_2 concentrations, this chemical reaction provides more metal vapor for nucleation, resulting in a higher initial number concentration (Fig. 5) than at lower CO_2 concentrations. Prior work has also shown that metallurgical chemistry strongly influences nucleation phenomenon and the resultant particle number concentration (Zimmer & Biswas, 2000). As previously demonstrated (Zimmer & Biswas, 2001), the dominant aerosol formation mechanisms for this GMAW alloy are nucleation followed by growth through coagulation.

Several specific observations can also be made for each shield gas condition with regard to the particle number concentration as a function of particle diameter (Fig. 4a–c). When comparing the Long DMA results for each shield gas condition, the total particle number concentration was similar with values ranging from 5.21×10^6 to 6.80×10^6 cm^{-3}. This appears reasonable in that the Long DMA (16.5 nm $< d_p <$ 562 nm) was configured to measure particle sizes found mainly within the accumulation mode. In contrast, the Nano DMA (4.53 nm $< d_p <$ 153 nm) was better equipped to measure particle sizes in the nucleation mode and the results revealed that an increase in CO_2

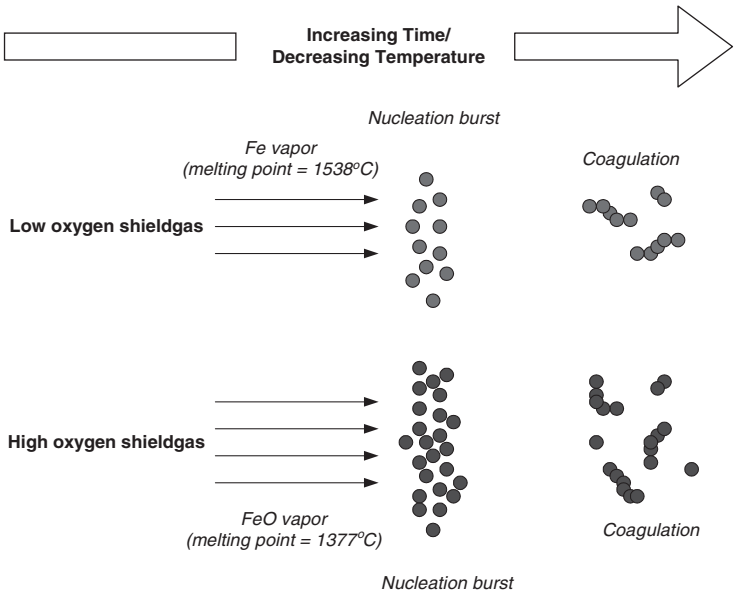

Fig. 5. Proposed mechanism to explain the differences in the particle size distribution results that were obtained for various shield gas compostions.

resulted in an increase in the particle number concentration within this size range. For example, when comparing the Nano DMA results for particle diameters less than 16.5 nm, the particle number concentration increased slightly from 8.12×10^4 cm^{-3} using a shield gas composed of 90% Ar/10% CO_2 to 1.43×10^5 cm^{-3} using a shield gas composed of 80% Ar/20% CO_2. Using 100% CO_2, the number concentration for particle diameters less than 16.5 nm increased markedly to 9.64×10^5 cm^{-3}, an order of magnitude increase when compared to the 90% Ar/10% CO_2 experimental results.

Several observations can be made regarding the geometric mean particle diameter and geometric standard deviation when weighted by number (Fig. 4a and b). The experimental results using the Long DMA revealed that both the geometric mean particle diameter and standard deviation increased with increasing CO_2 shield gas content. For example, the geometric mean particle diameter increased from 113.3 nm ($\sigma_g = 2.09$) using a 90% Ar/10% CO_2 shield gas to 118.7 nm ($\sigma_g = 2.13$) using a 80% Ar/20% CO_2 shield gas. Using 100% CO_2 shield gas, both the geometric mean particle diameter and standard deviation further increased to 123.7 nm and 2.34, respectively. These values represent average values from the replicate sample runs. The increase in the geometric standard deviation appears to relate to the presence of both an accumulation and nucleation mode. The Nano DMA results indicate that this trend became more pronounced and changed from 1.90 using a 90% Ar/10% CO_2 shield gas to 2.73 using 100% CO_2. The Nano DMA for the 100% CO_2 experimental runs revealed the presence of a distinct nucleation mode with the following particle size statistics for particle diameters in the range of 4.53–16.5 nm: N_{tot} of 1.08×10^6 cm^{-3}, d_{gm} of 9.63 nm, and σ_g of 1.41. It appears that an increase in CO_2 resulted in a larger concentration of nucleated particles. As a result, the particle size distribution revealed a distinct accumulation mode, as well as nucleation mode using 100% CO_2. In contrast, the particle size distribution for both the 90% Ar/10% CO_2 and 80% Ar/20% CO_2 shield gases produced a smaller number of particles during nucleation (Fig. 5).

A distinct accumulation mode was noted while the nucleation mode was not pronounced, because particles in the nucleation mode had been scavenged by larger particles in the accumulation mode at this residence time (i.e., 3.2 s).

The experimental results for 100% CO_2 shield gas (Fig. 4c) were plotted with a fitted bimodal particle size distribution (using a log-normal assumption) as a comparison (Fig. 3b). For Fig. 3b, the means of the Nano DMA results (4.53 nm $< d_p <$ 16.5 nm) were combined with the means from the Long DMA results (17.8 nm $< d_p <$ 562 nm). The bimodal distribution, determined using a trial and error method, revealed fitted particle size statistics that were quite similar to the experimental results for spray transfer. For example, experimental results for the nucleation mode, using the Nano DMA, compared reasonably well to the fitted results: $N_{\text{tot,experiment}} = 1.08 \times 10^6$ cm^{-3} versus $N_{\text{tot,theory}} = 1.1 \times 10^6$ cm^{-3}, $d_{\text{gm,experiment}} = 9.63$ nm versus $d_{\text{gm,theory}} = 10$ nm, $\sigma_{\text{g,experiment}} = 1.41$ versus $\sigma_{\text{g,theory}} = 1.5$. The experimental results for the accumulation mode, using the Long DMA, also compared reasonably well to the fitted results: $N_{\text{tot,experiment}} = 6.80 \times 10^6$ cm^{-3} versus $N_{\text{tot,theory}} = 5.5 \times 10^6$ cm^{-3}, $d_{\text{gm,experiment}} = 123.7$ nm versus $d_{\text{gm,theory}} = 141$ nm, $\sigma_{\text{g,experiment}} = 2.34$ versus $\sigma_{\text{g,theory}} = 2.5$.

3.3. The effect of shield gas composition on the particle size distribution of micrometer-sized aerosols (e.g., spatter)

It has been previously recognized that welding spatter contributes to the formation of sub-micrometer aerosols as a result of the evaporation of alloy vapors from the molten surface, and that an increase in oxidizing gases in the shield gas will increase spatter formation (Gray et al., 1982; Hewitt & Hirst, 1993). It is also thought that these aerosols are too large to contribute to the formation of a respirable aerosol (Gray, 1980a; Hewitt & Hirst, 1993). To characterize welding spatter, experiments were conducted to microscopically evaluate the welding spatter subject to changing shield gas and mass transfer conditions. Using a "cold finger" technique, welding spatter was collected at a distance of 5 cm from the arc using un-coated glass slides over a 15 s interval. Microscopic evaluation revealed the presence of spherically shaped particles with a diameter range of several to several hundred micrometers in diameter. Microscopic evaluation of these slides revealed no clearly observable differences among the various shield gas or mass transfer conditions. Aerosizer measurements were performed to quantitatively determine if the spatter particles contributed to a respirable welding aerosol.

Fig. 6 gives the particle size distribution measurements obtained while using a 90% Ar/10% CO_2 and 100% CO_2 shield gas. The following conditions were held constant: an extension height of 1.0 cm, an applied arc voltage was 20.5 V, and a shield gas flowrate of 0.3 cm^3 s^{-1}. Two replicate samples were collected for each experimental condition, and the bars represent the standard error associated with each particle-size bin. To adequately resolve the particle size distribution for this mode, particle diameters less than 1 μm are not shown. Measurements were collected on the arc centerline at a vertical distance of 19.2 cm, and the Aerosizer was set to dilute the number concentration of the aerosol by seven-fold. To determine if the Aerosizer measurements were accurate, an impactor with an aerodynamic cutoff of 5.2 μm was placed before the Aerosizer inlet to obtain fume measurements with/without an impactor. Based upon these results, each particle-size bin was shifted slightly by the ratio of the actual versus measured cutoff (actual ratio applied to each particle-size bin was 1.4).

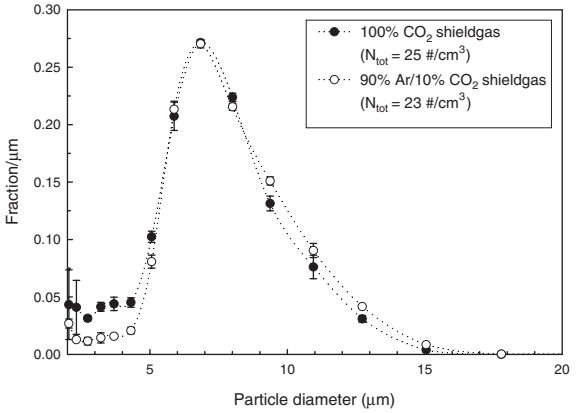

Fig. 6. Aerosizer results for the GMAW using a 90% Ar/10% CO_2 shield gas (hollow circles) and 100% CO_2 (darkened circles) shield gas at a sample height 19.2 cm above the arc centerline.

As shown in Fig. 6, welding spatter resulted in a respirable particle size distribution with a modal particle diameter of 6.8 μm for each shield gas condition. Interestingly, the distributions for both shield gas conditions are quite similar both with regard to the mode particle diameter and the total number concentration (23 cm^{-3} for a 90% Ar/10% CO_2 shield gas versus 25 cm^{-3} for a 100% CO_2 shield gas). Using information on the sample conditions, calculations were performed to estimate the loss of particles within the sample train (Baron, 1994). These results revealed that particle loss for larger particle diameters could be significant. For example, for a particle diameter of 10 μm, the loss of particles within the sample train was approximately 40%. As such, this experiment may not fully reveal the right-hand side of the distribution. However, general comparisons can be made with regard to the spatter and sub-micrometer aerosols. In comparing the distribution statistics from both the Aerosizer and the SMPS, the spatter aerosol is roughly five-orders of magnitude smaller with regard to particle number and two-orders of magnitude smaller with regard to particle mass. Therefore, although welding spatter contributes to a respirable aerosol, it is significantly less than that of the sub-micrometer aerosols.

References

Baron, P. A. (1994). *Aerosol Calculator* (Computer Spreadsheet). St. Paul, MN: TSI, Inc.

Biswas, P. (1993). Measurement of high-concentration and high-temperature aerosols. In: K. Willeke, & P. A. Baron (Eds.), *Aerosol Measurement* (pp. 705–714). New York, NY: Van Nostrand Reinhold.

Ferin, J., Oberdorster, G., Penney, D. P., Soderholm, S. C., Gelein, R., & Piper, H. C. (1990). Increased pulmonary toxicity of ultrafine particles? I. Particle clearance, translocation, morphology. *Journal of Aerosol Science*, *21*, 381–383.

Gray, C. N. (1980a). *Fume Formation in Electric Arc Welding*. Ph.D Thesis, University of Bradford, United Kingdom.

Gray, C. N. (1980b). Prediction of fume compositions in stainless steel metal inert gas welding. *The Welding Institute*, *Weld Pool Chemistry*, *and Metallurgy—International Conference*, London, 15–17 April.

Gray, C. N., & Hewitt, P. J. (1982). Control of particulate emissions from electric-arc welding by process modification. *Annals of Occupational Hygiene*, *25*, 431–438.

Gray, C. N., Hewitt, P. J., & Dare, P. R. M. (1982). New approach would help control weld fumes at source. *Welding Metal Fabrication*, *50*, 393–397.

Gray, C. N., Hewitt, P. J., & Hicks, R. (1980). The effect of oxygen on the rate of fume formation in metal inert gas welding arcs. *Weld Pool Chemistry and Metallurgy* (pp. 167–175). London: The Welding Institute.

Heile, R. R., & Hill, D. C. (1975). Particulate fume generation in arc welding processes. *Welding Journal*, *54*, 201s–210s.

Hewitt, P. J., & Hirst, A. A. (1993). A systems approach to the control of welding fumes at the source. *Annals of Occupational Hygiene*, *37*, 297–306.

Hilton, D. E., & Plumridge, P. N. (1991). Particulate fume generation during GMAW and GTAW. *Welding and Metal Fabrication*, *59*, 555–562.

Hinds, W. C. (1999). *Aerosol Technology* (pp. 206–216). New York: Wiley.

Ma, J., & Apps, R. L. (1982). MIG transfer discovery of importance to industry. *Welding and Metal Fabrication*, *10*, 307–316.

NIOSH (1988). National Institute for Occupational Safety and Health, *NIOSH Criteria for a Recommended Standard*: *Welding*, *Brazing*, *and Thermal Cutting*. DHHS (NIOSH) Publication No. 88-110, Cincinnati, OH.

Oberdorster, G., Ferin, J., Penney, D. P., Soderholm, S. C., Gelein, R., & Piper, H. C. (1990). Increased pulmonary toxicity of ultrafine particles? II. Lung lavage studies. *Journal of Aerosol Science*, *21*, 384–387.

Takenaka, S., Dornhofer-Takenaka, H., & Muhle, H. (1986). Aveolar distribution of fly ash and titanium dioxide after long-term inhalation by Wistar rats. *Journal of Aerosol Science*, *17*, 361–364.

Zimmer, A. T. (2000). *Aerosol formation mechanisms*, *metallurgical aspects*, *and engineering control of fumes generated from gas metal arc welding operations*. Ph.D. thesis, University of Cincinnati, Cincinnati, OH.

Zimmer, A. T., & Biswas, P. (2000). Mechanistic understanding of aerosol emissions from a brazing operation. *American Industrial Hygiene Association, Journal*, *16*, 351–361.

Zimmer, A. T., & Biswas, P. (2001). Characterization of aerosols resulting from arc welding processes. *Journal of Aerosol Science*, *32*, 993–1008.